

Freiburg-THEP 00/17
TTP00-25
hep-ph/0012002
December 2000

Three-loop non-diagonal current correlators in QCD and NLO corrections to single-top-quark production

K.G. Chetyrkin^{a,b,‡} and M. Steinhauser^c

(a) Fakultät für Physik,
Universität Freiburg, D-79104 Freiburg, Germany

(b) Institut für Theoretische Teilchenphysik,
Universität Karlsruhe, D-76128 Karlsruhe, Germany

(c) II. Institut für Theoretische Physik,
Universität Hamburg, D-22761 Hamburg, Germany

Abstract

The non-diagonal correlators of vector and scalar currents are considered at three-loop order in QCD. The full mass dependence is computed in the case where one of the quarks is massless and the other one carries the mass M . As applications we consider the single-top-quark production via the process $q\bar{q} \rightarrow t\bar{b}$ and the decay rate of a charged Higgs into hadrons. In both cases the computed NLO corrections are shown to be numerically much less important than the leading ones.

[‡]Permanent address: Institute for Nuclear Research, Russian Academy of Sciences, 60th October Anniversary Prospect 7a, Moscow 117312, Russia.

1 Introduction

In high energy experiments where the center-of-mass energy, \sqrt{s} , is much larger than the mass of the quarks, M , the latter can often be neglected or an expansion in M/\sqrt{s} is sufficient to describe the experimental data. However, there are situations where the full dependence on M and \sqrt{s} is required. One can, e.g., think on the high precision which meanwhile has been reached at LEP (CERN), SLC (SLAC) or TEVATRON (Fermilab) or on situations where the center-of-mass energy is of the same order of magnitude as the quark masses. In particular for threshold phenomena the masses are important and the full dependence is desirable.

A variety of important observables can be described by the correlators of two currents with different tensorial structure. If the coupling of the currents to quarks is diagonal quantities like e^+e^- annihilation into hadrons and the decay of the Z boson are covered by the vector and axial-vector current correlators. Total decay rates of neutral CP even or CP odd Higgs bosons can be obtained with the help of the scalar and pseudo-scalar current densities, respectively. For these cases the full mass dependence at order α_s^2 has been computed in [1] for the non-singlet and in [2] for the singlet correlators.

In this work we deal with three-loop correlators of currents which couple to two different quarks flavours: a massless one and one carrying the mass M .

The non-diagonal vector and axial-vector correlators describe properties connected to the W boson. The absorptive part of these correlators is directly related to the decay width of a (highly virtual) W boson into quark pairs and gluons. Of particular interest in this connection is the single-top-quark production via the process $q\bar{q} \rightarrow t\bar{b}$ [3, 4]. This is because the process directly probes the matrix element $|V_{tb}|$ — one of the few parameters of the Standard model not yet experimentally measured. The imaginary part of the transversal W boson polarization function constitutes a gauge invariant and finite contribution of $\mathcal{O}(\alpha_s^2)$ to the process.

As an application of the (pseudo-)scalar current correlator we consider the decay of a charged Higgs boson which occurs in extensions of the Standard Model. The corrections provided in this paper describe the total hadronic decay rate of such a boson (coupled to a massive and a massless quark).

2 Definitions

In the vector case the polarization function is defined through

$$\left(-q^2 g_{\mu\nu} + q_\mu q_\nu\right) \Pi^v(q^2) + q_\mu q_\nu \Pi_L^v(q^2) = i \int dx e^{iqx} \langle 0 | T j_\mu^v(x) j_\nu^{v\dagger}(0) | 0 \rangle, \quad (1)$$

with $j_\mu^v = \bar{\psi}_1 \gamma_\mu \psi_2$. Only the transversal part $\Pi^v(q^2)$ will be considered in the following. The definition of the scalar polarization function reads

$$q^2 \Pi^s(q^2) = i \int dx e^{iqx} \langle 0 | T j^s(x) j^{s\dagger}(0) | 0 \rangle, \quad (2)$$

with $j^s = (m(\mu)/M)\bar{\psi}_1\psi_2$ where $m(\mu)$ is the $\overline{\text{MS}}$ quark mass and M is its pole mass. Throughout this paper we consider anti-commuting γ_5 . This is justified because only non-singlet diagrams contribute (ψ_1 is supposed to be different from ψ_2). Thus, within perturbation theory, the axial-vector and pseudo-scalar correlators coincide with the vector and scalar ones, respectively.

We consider only the case where one of the quarks is massive. Thus we will identify ψ_1 with q , the massless quark, and ψ_2 with Q which is supposed to be a heavy quark of mass M . Furthermore it is convenient to introduce the dimensionless variable

$$z = \frac{q^2}{M^2}, \quad (3)$$

where M refers to the pole mass. For the overall normalization of $\Pi^\delta(q^2)$ ($\delta = v, s$) we adopt the QED-like conditions $\Pi^\delta(0) = 0$.

The physical observables $R(s)$ are related to $\Pi(q^2)$ through

$$R^v(s) = 12\pi \text{Im} \left[\Pi^v(q^2 = s + i\epsilon) \right], \quad (4)$$

$$R^s(s) = 8\pi \text{Im} \left[\Pi^s(q^2 = s + i\epsilon) \right], \quad (5)$$

where the use of the variables

$$x = \frac{M}{\sqrt{s}}, \quad v = \frac{1 - x^2}{1 + x^2}, \quad (6)$$

turns out to be useful to describe the high energy and threshold region, respectively.

The expansion of Π^δ in terms of α_s reads ($\delta = v, s$)

$$\Pi^\delta = \Pi^{(0),\delta} + \frac{\alpha_s^{(n_f)}(\mu)}{\pi} C_F \Pi^{(1),\delta} + \left(\frac{\alpha_s^{(n_f)}(\mu)}{\pi} \right)^2 \Pi^{(2),\delta} + \mathcal{O}(\alpha_s^3). \quad (7)$$

It is convenient to decompose the three-loop term according to the colour structure

$$\Pi^{(2),\delta} = C_F^2 \Pi_{FF}^{(2),\delta} + C_A C_F \Pi_{FA}^{(2),\delta} + C_F T n_l \Pi_{FL}^{(2),\delta} + C_F T \Pi_{FH}^{(2),\delta}, \quad (8)$$

where analogous formulae hold for $R(s)$. In Eq. (8) $\Pi_{FF}^{(2),\delta}$ corresponds to the abelian part already present in QED whereas the non-abelian structure is contained in $\Pi_{FA}^{(2),\delta}$. The remaining two structures correspond to the fermionic contributions where n_l counts the number of massless quarks and $n_f = n_l + 1$ is the total number of active quark flavours.

3 Calculation

A complete analytical computation of $\Pi^\delta(q^2)$ at three-loop order or its imaginary part is currently not feasible. The method we use for the computation of the diagrams is based on conformal mapping and Padé approximation [5, 6, 1, 2]. It allows for the computation of a semi-numerical approximation for $\Pi^\delta(q^2)$. The aim is the reconstruction of the function $\Pi^\delta(q^2)$ from the knowledge of some moments for $z \rightarrow 0$ and $z \rightarrow -\infty$ and additional partial information about the behaviour of $R(s)$ close to the threshold, i.e. for $s \rightarrow M^2$. Thus let us in the following briefly discuss the different kinematical regions.

Expansions for small and large external momentum

The number of diagrams which contribute at one-, two- and three-loop order is relatively small and amounts to one, three and 31, respectively. Nevertheless we used **GEFICOM** [7] for the automatic computation. **GEFICOM** uses **QGRAF** [8] for the generation of the diagrams. In case an asymptotic expansion has to be applied **LMP** [9] or **EXP** [10] are used for the generation of the sub-diagrams. The occurring vacuum diagrams are passed to **MATAD** [11] and the massless propagator type diagrams are evaluated with **MINCER** [12]. More details on the automatic computation of Feynman diagrams can be found in [13].

We have been able to compute seven terms for small and eight terms for large external momentum q both for the vector and scalar correlators of Eqs. (1) and (2), respectively. This means expansion coefficients up to order z^6 , respectively, $1/z^7$ are available for the Padé procedure. The analytical results are rather bulky and will be published elsewhere.

Threshold behaviour

The Born results for the vector and scalar spectral functions are proportional to v^2 in the limit $v \rightarrow 0$ as can be seen for the exact results

$$R^{(0),v}(s) = \frac{N_c}{2} (1 - x^2)^2 (2 + x^2) , \quad (9)$$

$$R^{(0),s}(s) = N_c (1 - x^2)^2 . \quad (10)$$

Also the corrections of order α_s to R^v and R^s are known [14, 15, 16, 17, 18] and a similar threshold behaviour is observed: the spectral functions vanish like v^2 (modulo powers of $\ln v$). This is valid in every order in α_s as follows from Heavy Quark Effective Theory (HQET) [19]. Actually the latter can be used to obtain the leading threshold behaviour of $R^v(s)$ and $R^s(s)$ at $\mathcal{O}(\alpha_s^2)$ from the corresponding correlators in HQET. In particular, the renormalization group equation in the effective theory is used to get the leading logarithmic behaviour at order α_s^2 . Afterwards the decoupling relation between the currents in the full and effective theory [20, 21, 22] is exploited to get the information about $R^v(s)$ and $R^s(s)$. For $\mu^2 = M^2$ our results read

$$\begin{aligned} R^{v,thr} = N_c v^2 & \left\{ 6 + \frac{\alpha_s^{(n_f)}(M)}{\pi} C_F \left(\frac{27}{2} + 12\zeta_2 - 9 \ln 2 - 9 \ln v \right) \right. \\ & + \left(\frac{\alpha_s^{(n_f)}(M)}{\pi} \right)^2 \left[C_F^2 \left(c_{FF}^v + \left(-\frac{147}{8} - 30\zeta_2 + \frac{27}{2} \ln 2 \right) \ln v + \frac{27}{4} \ln^2 v \right) \right. \\ & + C_A C_F \left(c_{FA}^v + \left(-\frac{423}{8} - 19\zeta_2 + \frac{33}{2} \ln 2 \right) \ln v + \frac{33}{4} \ln^2 v \right) \\ & + C_F T n_l \left(c_{FL}^v + \left(\frac{39}{2} + 8\zeta_2 - 6 \ln 2 \right) \ln v - 3 \ln^2 v \right) \\ & \left. \left. + C_F T \left(\frac{133}{8} - 10\zeta_2 \right) \right] \right\} , \quad (11) \end{aligned}$$

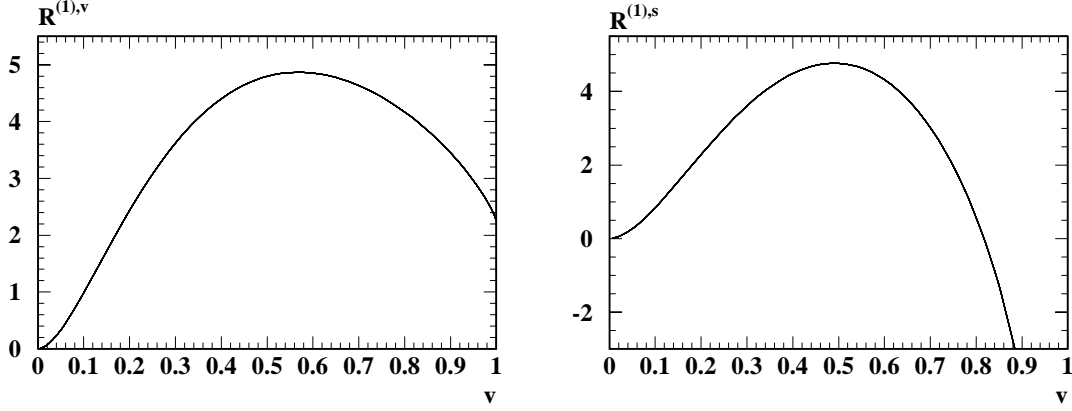


Figure 1: $R^{(1),v}(s)$ and $R^{(1),s}(s)$ as a function of v .

$$\begin{aligned}
R^{s,thr} = & N_c v^2 \left\{ 4 + \frac{\alpha_s^{(n_f)}(M)}{\pi} C_F (13 + 8\zeta_2 - 6 \ln 2 - 6 \ln v) \right. \\
& + \left(\frac{\alpha_s^{(n_f)}(M)}{\pi} \right)^2 \left[C_F^2 \left(c_{FF}^s + \left(-\frac{73}{4} - 20\zeta_2 + 9 \ln 2 \right) \ln v + \frac{9}{2} \ln^2 v \right) \right. \\
& + C_A C_F \left(c_{FA}^s + \left(-\frac{141}{4} - \frac{38}{3} \zeta_2 + 11 \ln 2 \right) \ln v + \frac{11}{2} \ln^2 v \right) \\
& + C_F T n_l \left(c_{FL}^s + \left(13 + \frac{16}{3} \zeta_2 - 4 \ln 2 \right) \ln v - 2 \ln^2 v \right) \\
& \left. \left. + C_F T \left(\frac{727}{36} - 12\zeta_2 \right) \right] \right\}, \tag{12}
\end{aligned}$$

with $\zeta_2 = \pi^2/6$. The constants $c_{FF}^\delta, c_{FA}^\delta$ and c_{FL}^δ ($\delta = s, v$) are unknown. Note, however, that the leading term for the colour structure $C_F T$ is completely determined. In order to incorporate the available threshold information into our method one has to perform an analytical continuation of the expressions in Eqs. (11) and (12). Taking the logarithmic parts of Eqs. (11) and (12) one obtains the quadratic and cubic logarithms for the polarization functions. They can be incorporated into the Padé procedure [1].

4 Results and Applications

In a first step we want to discuss the results for the spectral functions R^v and R^s which essentially corresponds to the direct outcome of the Padé method. For the results we present in the following, those Padé approximants are chosen which contain for their construction at least terms of order z^5 and $1/z^5$ in the small and large momentum region, respectively. Furthermore we demand that the difference of the degree in the numerator and denominator is less or equal to two. In the numerical evaluations we specify $\mu^2 = M^2$.

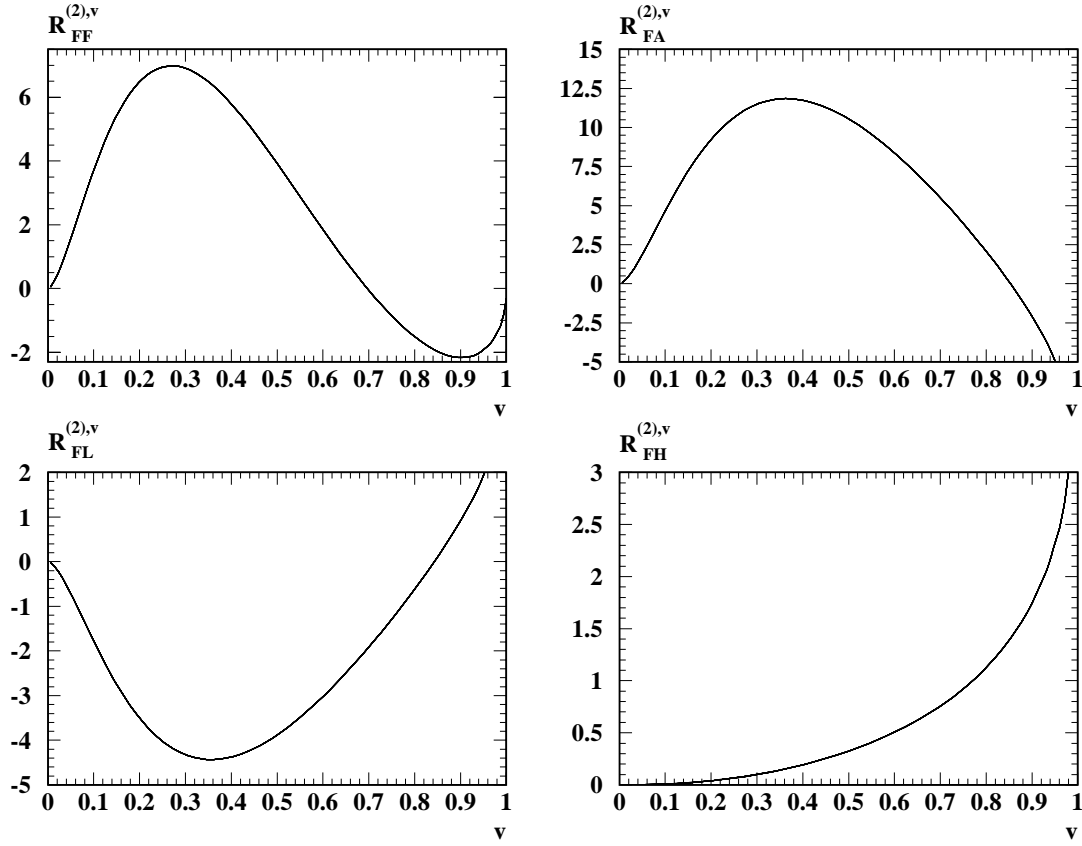


Figure 2: $R_{FF}^{(2),v}(s)$, $R_{FA}^{(2),v}(s)$, $R_{FL}^{(2),v}(s)$ and $R_{FH}^{(2),v}(s)$ as a function of v .

The analytical formulae which result from the semi-numerical Padé procedure are quite long. Thus we refrain from listing them explicitly. Instead, a typical representative for each colour structure can be found under the URL <http://www-ttp.physik.uni-karlsruhe.de/Progdata/ttp00-25>.

At order α_s the exact results are known. Thus it is instructive to make a comparison with the outcome of our semi-numerical method. In Fig. 1 roughly 15 Padé approximants are plotted together with the exact curves. Note that even for small values of v , where only the logarithmic parts of Eqs. (11) and (12) are incorporated in our method, no difference both between the individual Padé expression and the exact result is visible. This is quite promising for the $\mathcal{O}(\alpha_s^2)$ results. The corresponding curves are shown in Fig. 2 and Fig. 3 for the vector and scalar case, respectively. Again of the order of 15 Padé approximants are plotted and no difference is visible. We should note that due to our choice $\mu^2 = M^2$ in the high energy limit all curves tend to $\pm\infty$ except $R_{FF}^{(2),v}$ which reaches a constant for $v \rightarrow 1$. In particular, $R_{FA}^{(2),s}$ and $R_{FL}^{(2),s}$ tend to $+\infty$, respectively, $-\infty$. This is not visible in the figures as the corresponding range in v where the turn over takes place is beyond the resolution in the plots.

In order to get even more confidence in the results we plot in Fig. 4 $R_{FF}^{(2),v}(s)$ and

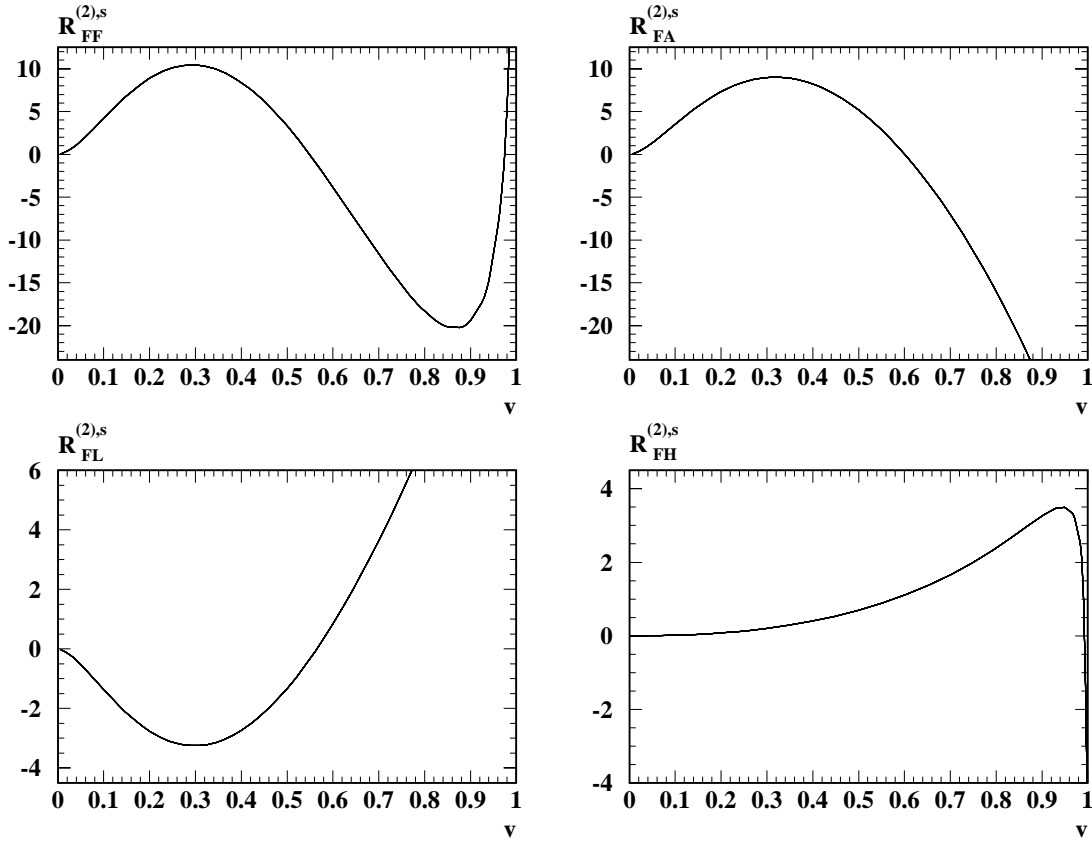


Figure 3: $R_{FF}^{(2),s}(s)$, $R_{FA}^{(2),s}(s)$, $R_{FL}^{(2),s}(s)$ and $R_{FH}^{(2),s}(s)$ as a function of v .

$R_{FF}^{(2),s}(s)$ as a function of x . Expressed in this variable the high energy region gets more spread. Thus a sensible comparison with the expansion terms can be performed. The dashed curves correspond to the analytical expressions obtained via asymptotic expansion containing the terms up to order $1/z^7$. Excellent agreement with the semi-numerical results is observed up to $x \approx 0.5$ for the vector case and $x \approx 0.7$ for the scalar case which corresponds to $v \approx 0.60$ and $v \approx 0.34$, respectively. This is a strong consistency check for the Padé method.

Single-top-quark production

As a first application we want to discuss the single-top-quark production via the process $q\bar{q} \rightarrow t\bar{b}$. Some sample diagrams are plotted in Fig. 5.

The corrections of order α_s to the (total) single-top-quark production rate are quite large. They amount to about 54% and 50% for Tevatron and LHC energies, respectively [23], where 18%, respectively, 17% arise from the final state corrections. This calls for a complete $\mathcal{O}(\alpha_s^2)$ calculation. In this letter we want to do a first step and consider the leading term in the large- N_c expansion.

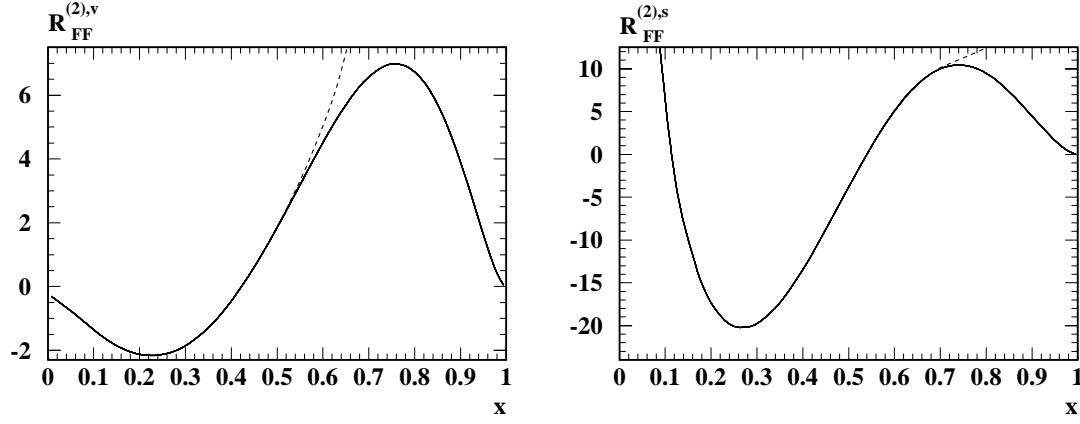


Figure 4: $R_{FF}^{(2),v}(s)$ and $R_{FF}^{(2),s}(s)$ as a function of x (full line). The dashed curves correspond to the high-energy results obtained via asymptotic expansion including terms up to order $1/z^7$.

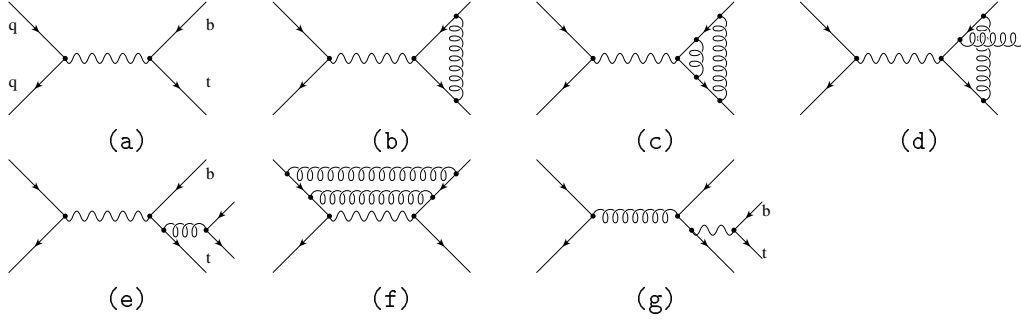


Figure 5: Sample diagrams contributing to the process $q\bar{q} \rightarrow t\bar{b}$. The wavy and loopy lines represent W bosons and gluons, respectively.

At $\mathcal{O}(\alpha_s)$ there is no interference between the initial and final state radiation. Thus it is possible to write the differential cross section in factorized form

$$\frac{d\sigma}{dq^2}(p\bar{p} \rightarrow t\bar{b} + X) = \sigma(p\bar{p} \rightarrow W^* + X) \frac{\text{Im} \Pi_W(q^2, M_t^2, M_b^2)}{\pi(q^2 - M_W^2)^2}, \quad (13)$$

where Π_W corresponds to the transversal part of the W boson correlator and is connected to the vector correlator of Eq. (1) through

$$\Pi_W(q^2) = \sqrt{2}G_F M_W^2 |V_{tb}|^2 q^2 \Pi^v(q^2). \quad (14)$$

Due to interference diagrams between the initial and final state (c.f. Fig. 5(f)) Eq. (13) does not hold at α_s^2 . However, those contributions are suppressed by at least a factor $1/N_c^2$ in large N_c limit as compared to the diagrams in Fig. 5(c)–(e). The latter, together with the contributions in Fig. 5(a) and (b), are covered by Eqs. (13) and (14).

At order α_s^2 there are also diagrams like the one in Fig. 5(g) which appear for the first time. In principle they lead to the same final state as the diagram in Fig. 5(e). However, one has to note that the W boson generating the top and bottom quark is radiated from a light quark flavour. Furthermore, compared to the diagram in Fig. 5(c) these contributions are only suppressed by a factor $1/N_c$ and not by $1/N_c^2$ like the diagram in Fig. 5(f).

Thus, if we restrict ourselves to the leading term in $1/N_c$ it is possible to use the results for R^v obtained above in combination with Eq. (13) to perform a theoretical analysis of the order α_s^2 to the single-top-quark production in the large- N_c limit. In order to obtain the total cross section the corresponding parton distribution functions would be needed to the same order.

The production cross-section of the virtual W^* boson is identical to that of the Drell-Yan process $q\bar{q} \rightarrow e\bar{\nu}_e$. The latter is known to $\mathcal{O}(\alpha_s^2)$ from Ref. [24]. Thus we can take the proper ratios to make predictions in the large- N_c limit at NNLO free from any dependence on parton distribution functions. As an example, we consider

$$\begin{aligned} \frac{\frac{d\sigma}{dq^2}(pp \rightarrow W^* \rightarrow tb)}{\frac{d\sigma}{dq^2}(pp \rightarrow W^* \rightarrow e\nu_e)} &= \frac{\text{Im}[\Pi_{tb}(q^2)]}{\text{Im}[\Pi_{e\nu}(q^2)]} \\ &= N_c |V_{tb}|^2 R^v(s). \end{aligned} \quad (15)$$

To get an impression of the numerical significance we plot in Fig. 6 the LO, NLO and NNLO result of $R^v(s)$ in the range $\sqrt{s} = 200 \dots 400$ GeV. For the numerical values we choose $M_t = 175$ GeV and $\alpha_s(M_Z) = 0.118$. Whereas the $\mathcal{O}(\alpha_s)$ corrections are significant there is only a moderate contribution from the order α_s^2 terms. In the range in q^2 shown in Fig. 6 they are below 1% of the Born result. Note that the NNLO correction to the Drell-Yan process are also small and amount to at most a few percent (see e.g. [25]). Thus, in case there is no kinematical magnification for the diagrams in Fig. 5(f) and (g) we can conclude that the radiative corrections to the single-top-quark production via the process $q\bar{q} \rightarrow t\bar{b}$ are well under control.

Decay rate of a charged Higgs

Theories beyond the SM are usually characterized by an enlarged Higgs sector and may allow for different quantum numbers of the Higgs bosons. For example, one of the most appealing extensions of the SM, the Minimal Supersymmetric Standard Model (MSSM), contains two complex iso-doublets with opposite hyper-charge (see e.g. [26]), resulting in five mass eigenstates of (pseudo-)scalar physical Higgs fields: two neutral CP-even (H^0 and h^0), one neutral CP-odd (A) and two charged (H^\pm) Higgs bosons.

Let us consider a generic charged Higgs boson coupled to fermions through

$$\mathcal{L}_{H^+ D \bar{U}} = (\sqrt{2} G_F)^{1/2} H^+ J_{H^+}, \quad (16)$$

where the corresponding quark current is given by

$$J_{H^+} = \frac{m_U}{\sqrt{2}} \bar{U} [a(1 - \gamma_5) + b(1 + \gamma_5)] D. \quad (17)$$

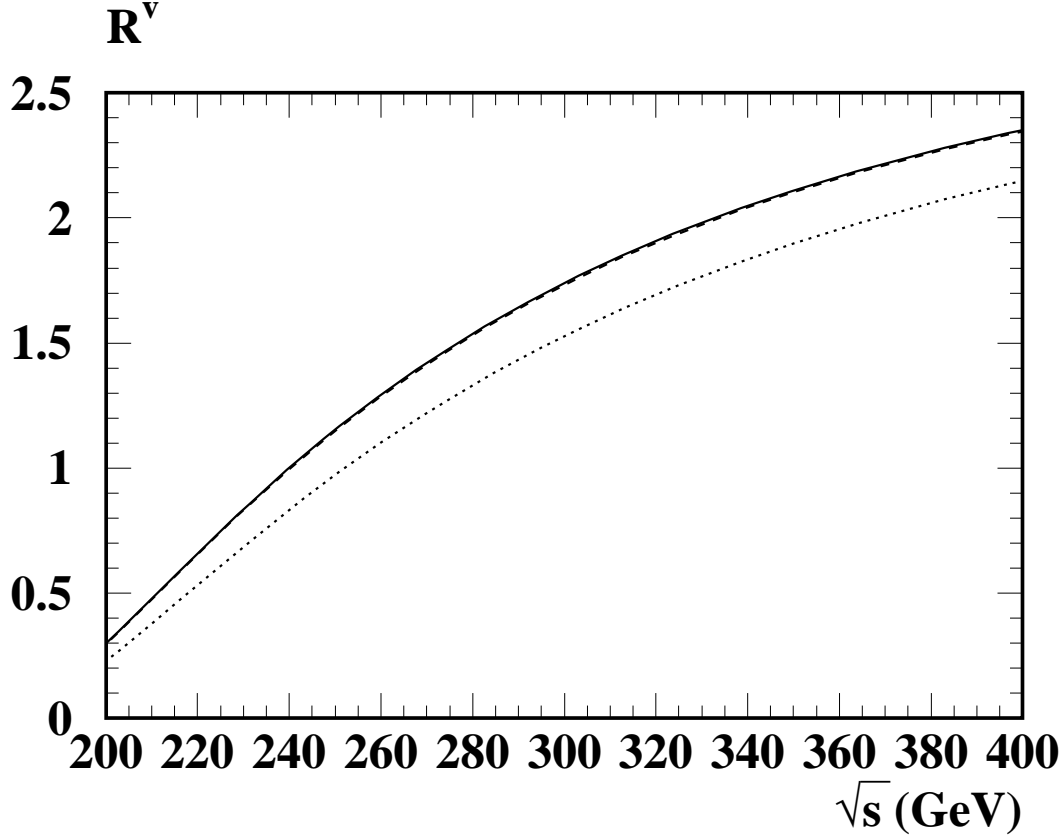


Figure 6: LO (dotted), NLO (dashed) and NNLO (solid) results of $R^v(s)$.

Here U and D represent generic up- and down-type quarks, respectively, with $\overline{\text{MS}}$ masses m_U and $m_D = 0$. We only consider H^+ as for H^- the formulae are analogues. The parameters a and b are model dependent and are left unspecified.

The decay rate of the Higgs boson H^+ into quarks and gluons can be written in the form

$$\Gamma(H^+ \rightarrow U\bar{D}) = \sqrt{2}G_F M_{H^+} \text{Im} [\Pi_H(M_{H^+}^2)] , \quad (18)$$

where M_U is the pole quark mass and $\Pi_H(q^2)$ is given by

$$q^2 \Pi_H(q^2) = \int dx e^{iqx} \langle T J_H^+(x) J_H^-(0) \rangle = (a^2 + b^2) q^2 \Pi^s(q^2) , \quad (19)$$

Thus, we arrive at the following expression for the hadronic decay rate of the charged Higgs boson

$$\Gamma(H^+ \rightarrow U\bar{D}) = \frac{\sqrt{2}G_F}{8\pi} M_{H^+} (a^2 + b^2) R^s(M_{H^+}^2) . \quad (20)$$

In Fig. 7 $R^s(M_{H^+}^2)$ is plotted at LO, NLO and NNLO. Again it turns out that the radiative corrections are well under control as order α_s^2 terms contribute at most of the order of 1%.

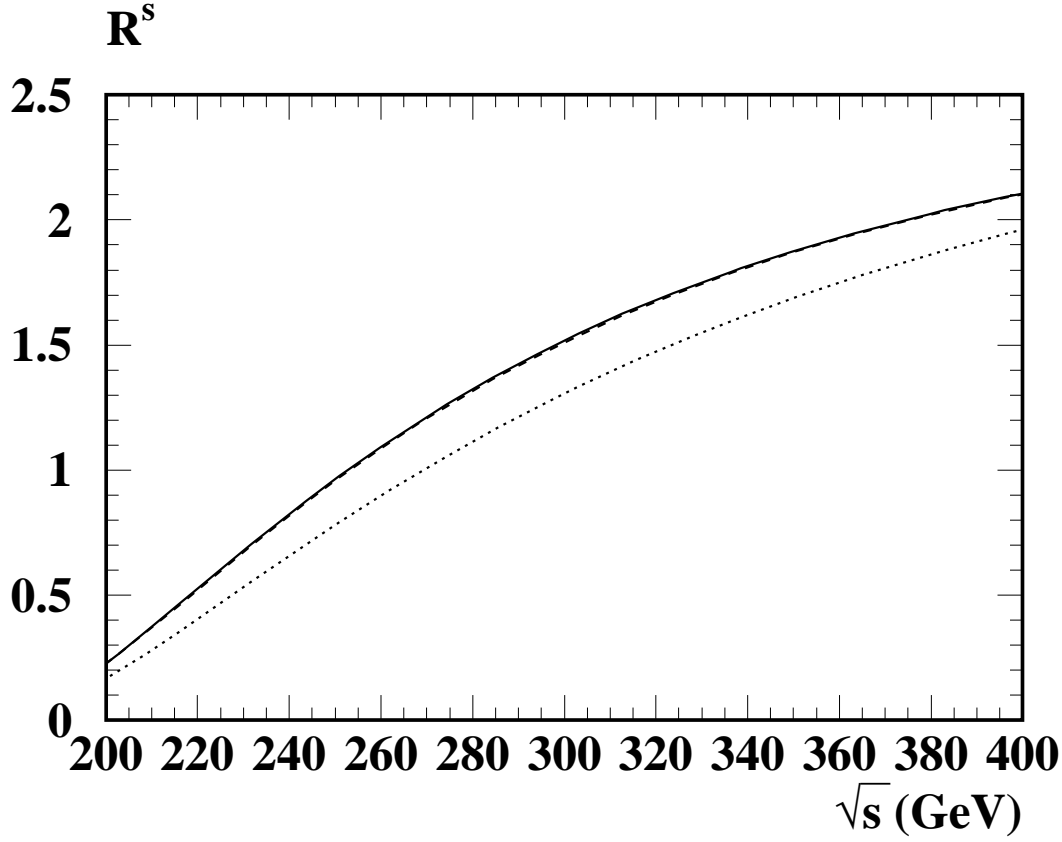


Figure 7: LO (dotted), NLO (dashed) and NNLO (solid) results of $R^s(s)$, $M = M_t = 175$ GeV.

5 Conclusions

We have computed the non-diagonal correlators of vector and scalar currents at order α_s^2 in the case of the currents composed from a massless and a massive quark field. Our main theoretical tools have been the asymptotic expansions in the large and small momentum region as well as some information about the threshold behaviour provided by HQET.

The obtained results for the case of the (axial-)vector correlator constitute an important ingredient of the full calculation of next-to-next-to-leading $\mathcal{O}(\alpha_s^2)$ correction to the single-top-quark production via the process $q\bar{q} \rightarrow t\bar{b}$. Such a calculation is required for an accurate extraction of the matrix element $|V_{tb}|$ from experiment.

We have used the results for the (pseudo-)scalar correlator in order to obtain the $\mathcal{O}(\alpha_s^2)$ decay rate of a charged (pseudo-)scalar Higgs boson to hadrons.

Acknowledgments

The authors are grateful to A. Grozin, J.H. Kühn and V.A. Smirnov for useful discussions and advice.

This work was supported in part by the *DFG DFG-Forschergruppe “Quantenfeldtheorie, Computeralgebra und Monte-Carlo-Simulation”* (contract FOR 264/2-1) and by SUN Microsystems through Academic Equipment Grant No. 14WU0148.

References

- [1] K.G. Chetyrkin, J.H. Kühn, and M. Steinhauser, *Phys. Lett. B* **371** (1996) 93; *Nucl. Phys. B* **482** (1996) 213; *Nucl. Phys. B* **505** (1997) 40.
- [2] K.G. Chetyrkin, R. Harlander, and M. Steinhauser, *Phys. Rev. D* **58** (1998) 014012.
- [3] S. Cortese and R. Petronzio, *Phys. Lett. B* **253** (1991) 494.
- [4] T. Stelzer and S. Willenbrock, *Phys. Lett. B* **357** (1995) 125.
- [5] J. Fleischer and O.V. Tarasov, *Z. Phys. C* **64** (1994) 413.
- [6] D.J. Broadhurst, J. Fleischer, and O.V. Tarasov, *Z. Phys. C* **60** (1993) 287; P.A. Baikov and D.J. Broadhurst, *4th International Workshop on Software Engineering and Artificial Intelligence for High Energy and Nuclear Physics (AIHENP95)*, Pisa, Italy, 3-8 April 1995. Published in Pisa AIHENP (1995) 167.
- [7] K.G. Chetyrkin and M. Steinhauser, unpublished.
- [8] P. Nogueira, *J. Comput. Phys.* **105** (1993) 279.
- [9] R. Harlander, Ph. D. thesis, University of Karlsruhe (Shaker Verlag, Aachen, 1998).
- [10] T. Seidensticker, Diploma thesis (University of Karlsruhe, 1998), unpublished.
- [11] M. Steinhauser, Report Nos.: DESY 00-124, TTP00-14, hep-ph/0009029, *Comp. Phys. Comm.* (in press).
- [12] S.A. Larin, F.V. Tkachov, and J.A.M. Vermaseren, Rep. No. NIKHEF-H/91-18 (Amsterdam, 1991).
- [13] R. Harlander and M. Steinhauser, *Prog. Part. Nucl. Phys.* **43** (1999) 167.
- [14] K. Schilcher, M.D. Tran, and N.F. Nasrallah, *Nucl. Phys. B* **181** (1981) 91; (E) **B 187** (1981) 594.
- [15] D.J. Broadhurst, *Phys. Lett. B* **101** (1981) 423.
- [16] T.H. Chang, K.J. Gaemers, and W.L. van Neerven, *Nucl. Phys. B* **202** (1982) 407.

- [17] L.J. Reinders, H. Rubinstein, and S. Yazaki, *Phys. Lett.* **B 97** (1980) 257, (E) **B100** (1981) 519, **B 103** (1981) 35.
- [18] A. Djouadi and P. Gambino, *Phys. Rev.* **D 49** (1994) 3499.
- [19] See, e.g. A.G. Grozin, *Lectures on perturbative HQET 1*, Report No.: hep-ph/0008300;
A.V. Manohar and M.B. Wise, *Heavy quark physics*, Cambridge University Press (2000).
- [20] X. Ji and M.J. Musolf, *Phys. Lett.* **B 257** (1991) 409;
D.J. Broadhurst and A.G. Grozin, *Phys. Lett.* **B 267** (1991) 105;
V. Giménez, *Nucl. Phys.* **B 375** (1992) 582.
- [21] D.J. Broadhurst and A.G. Grozin, *Phys. Rev.* **D 52** (1995) 4082.
- [22] A.G. Grozin, *Phys. Lett.* **B 445** (1998) 165.
- [23] M.C. Smith and S. Willenbrock, *Phys. Rev.* **D D54** (1996) 6696.
- [24] R. Hamberg, W. van Neerven, and T. Matsuura, *Nucl. Phys.* **B 359** (1991) 343;
W. van Neerven and E. Zijlstra, *Nucl. Phys.* **B 382** (1992) 11.
- [25] A.D. Martin, R.G. Roberts, W.J. Stirling, and R.S. Thorne, Report Nos.: DTP-00-38, RAL-TR-2000-028, hep-ph/0007099.
- [26] J.F.Gunion, H.E.Haber, G.Kane, and S.Dawson, *The Higgs Hunter's Guide*, Addison Wesley 1990.